Available online at www.sciencedirect.com

jmr&t Journal of Materials Research and Technology

journal homepage: www.elsevier.com/locate/jmrt

Sustainable cementitious composites with 30% porosity and a compressive strength of 30 MPa

Siyu Wu [1], Kebede Alemayehu Moges [1], Prabhat Vashistha, Sukhoon Pyo*

Department of Urban and Environmental Engineering, Ulsan National Institute of Science and Technology (UNIST), Ulsan 44919, Republic of Korea

ARTICLE INFO

Article history:
Received 13 May 2023
Accepted 4 July 2023
Available online 7 July 2023

Keywords:
High-strength foamed geopolymer
Lime mud
Fly ash
Porosity
CO_2 emissions

ABSTRACT

Many researchers have tried to increase the porosity of cement-based materials for different applications, but a limitation of the existing technology is that it is difficult to achieve more than 30 MPa compressive strength for materials that have a porosity of more than 30%. To overcome the decrease in compressive strength, some studies have developed fly ash-based foam geopolymers with silica fume as the foaming agent. However, this material requires heat curing and has a rapid setting problem. Therefore, the present study aimed to develop a material that can maintain compressive strength above 30 MPa while increasing the porosity to 30%, solving the curing problem, and extending the setting time. This study proposes a sustainable material design based on the concept of limestone calcined clay cement (LC^3) and a fly ash–based foamed geopolymer. The results show that the proposed material can generate porosity of more than 30% and maintain a compressive strength above 30 MPa while the rapid setting and curing limitation problems are solved. Moreover, the developed cementitious composite was proven to reduce CO_2 emissions by 31.91% compared to conventional construction materials, which highlights that the newly developed material can be classified as a low carbon construction material.

1. Introduction

Numerous researchers have attempted to increase the porosity of construction materials appropriately for diverse applications, such as thermal insulation, noise insulation, and vibration reduction [1–3]. In some studies, a physical method was used by adding an air-entraining agent to increase the porosity to more than 20%, but the compressive strength decreased to less than 30 MPa because the increased porosity using air-entraining agents without increasing strength of the matrix deteriorated the overall strength of construction materials [4–7]. The other method is the chemical method, which follows the reaction among hydrogen peroxide, sodium hypochlorite, Al, Si, and alkaline solution to generate pores [8]. Based on these reactions, some researchers have developed a fly ash (FA)–based geopolymer with silica fume (SF) as the foaming agent [9], which can increase the porosity to 20% while maintaining the compressive strength at 30 MPa with the appropriate SF content. However, this geopolymer has several limitations, such as requiring heat curing and having a rapid setting time [10,11], which are difficult to practically apply in construction.

The common method for developing construction materials with appropriate porosity around 15% is based on conventional cement-based materials with an air-entraining

* Corresponding author.
E-mail address: shpyo@unist.ac.kr (S. Pyo).
[1] These authors contributed equally to the present study.
https://doi.org/10.1016/j.jmrt.2023.07.036

agent while maintaining a compressive strength around 20 MPa. However, the CO_2 emissions from cement clinker production account for 7%–10% of the global CO_2 emissions [12]. Therefore, some studies have focused on reducing cement usage by employing supplementary cementitious materials (SCM) to replace cement. Materials that cause fewer CO_2 emissions during the production process were chosen as the SCM. Calcined clay needs only half of the calcination temperature of cement clinker production, and limestone powder does not need calcination; therefore, these two materials have lower CO_2 emissions than cement clinker. Limestone calcined clay cement (LC^3), a sophisticated low-carbon construction material, was developed based on this concept [13]. LC^3 has been widely used in construction because it is easy for untrained workers to use it as cement without particular health and safety issues [13]. There are some application examples based on LC^3, such as the Swiss Embassy building in Delhi, the street pavement on the Central University "Marta Abreu" of Las Villas campus in Cuba, and a house building in Santa Clara in the United States. In LC^3, 60% of the cement can be replaced with calcined clay and limestone powder, while the compressive strength reaches 50 MPa [14]; however, limestone powder production processing still consumes energy and generates CO_2. Therefore, it is better to find a kind of industrial byproducts that have the similar chemical components to replace limestone powder.

Lime mud (LM) is a type of industrial waste from the papermaking process that mainly consists of calcium carbonate. Existing studies have shown that solid waste from the papermaking industry causes severe environmental pollution problems, such as groundwater pollution and vegetation damage [15–18]. Therefore, some studies have focused on applying solid waste, such as LM, to construction materials. However, a previous study [19] showed that the addition of LM decreased the compressive strength due to LM's low reactivity. In contrast, it was revealed that the appropriate replacement ratio in a mortar improved the compressive strength and prolonged the setting time compared to that for normal mortar [20].

Metakaolin (MK) is a calcined, high purity kaolinitic clay used as supplementary cementitious materials, so it contributes to the pozzolanic reaction in cementitious composites. In LC^3, the calcined clay can have less than 40% kaolinite content, which can also participate in the pozzolanic reaction, and the 28-day compressive strength of LC^3 can achieve more than 45 MPa [21]. Previous studies showed that the alumina in MK or low kaolinite calcined clay in LC^3 could react with limestone powder to form fillers in the mortar matrix to improve compressive strength [14,22]. However, no study has investigated whether LM is reactive with MK in LC^3 paste. Therefore, this study attempts to address this gap in the literature. This study also aims to overcome the significant compressive strength decrease, curing problem, and rapid setting in the literature by developing a high-volume lime mud–based cementless binder based on a combination of LC^3 and a foamed fly ash–based geopolymer to alleviate the environmental burden [23]. Because the kaolinite content of the calcined clay in LC^3 is lower than that of MK [14], FA and SF replace part of MK to decrease the kaolinite content. In this study, it is called lime mud metakaolin geopolymer cement (LMMGC).

This study examines the properties of the proposed LMMGC and mainly aims to develop an LMMGC that has 30% porosity with compressive strength above 30 MPa. Different LM content was used to replace limestone powder in the mixture, and the foaming fly-ash geopolymer replaced part of the metakaolin to reduce the kaolinite content and to generate pores. The reaction between metakaolin and LM was investigated with thermogravimetric analysis (TGA), and the setting time was measured with calorimetry and setting time tests. The compressive strength and porosity of the LMMGC specimens were evaluated. Finally, the CO_2 emissions of the LMMGC were evaluated to highlight that it is a low-carbon construction material.

2. Materials and methods

2.1. Raw materials

The specimens used in this study were made from Type I cement and natural river sand, MK, FA, SF, and LM. A commercial water glass (WG) with a specific gravity 1.5 was used as an activator for the geopolymer part. A polycarboxylate-based superplasticizer was also used to compensate for the decrease in fresh mortar flowability resulting from the use of LM and other fine powder materials.

The cement was purchased from Halla Cement in South Korea and has a surface area of 1.44 m^2/cm^3 and a mean particle size of 11.03 μm, and MK was purchased from Nycontech in China and has a surface area of 2.9 m^2/cm^3 and a mean particle size of 3.19 μm. FA was purchased from Maxcon in South Korea and SF from Elkem in South Korea. Moorim Paper Industry in South Korea supplied the LM. Moorim Paper Industry in South Korea supplied the LM. LM is solid waste produced during the alkali recycling process in the papermaking process. LM has a moisture content of 56.3%; therefore, it was completely dried in an oven at 80 °C to remove the moisture and reduce agglomeration. The cement used has a density of 3.14 g/cm^3, while the densities of metakaolin, silica fume, fly ash, lime mud, and river sand are 2.6, 2.2, 2.1, 2.7, and 2.65 g/cm^3, respectively. The chemical composition of the binding materials, which was obtained with X-ray fluorescence analysis (XRF; T8 tiger, USA), is shown in Table 1. It should be noted that LM has 90.4 wt% of CaO, which was the result of a causticization reaction.

2.2. Specimen preparation

Three specimens were prepared using a water-to-binder ratio of 0.5 and a sand-to-binder ratio of 2.0 for each mixture. The mortars were prepared following ASTM 305 [24]. The superplasticizer used was 2% of the weight of the binder. As can be seen in the mix design presented in Table 2, the proportions of the materials were determined based on previous studies on LC^3 and low-carbon foamed materials [13,14]. The ratio of MK was 20%, which is half of that used in typical LC^3 cement because the kaolinite content in MK is almost twice that of calcined clay. Based on previous research on LC^3, cement and

Table 1 – Chemical composition of binding materials (wt%)

	CaO	SiO_2	Al_2O_3	Fe_2O_3	MgO	SO_3	Na_2O	K_2O	Others
Cement	64.1	17.8	4.4	3.7	3.3	3.9	0.5	1.4	1.0
Silica fume (SF)	0.1	97.3	0.1	0.2	0.4	0.9	–	–	1.0
Lime mud (LM)	90.4	0.8	0.5	0.9	1.4	1.3	2.5	0.1	2.1
Metakaolin (MK)	0.5	50.4	43.3	2.8	0.2	0.1	–	–	2.8
Fly ash (FA)	4.3	57.1	23.9	7.1	1.1	0.6	1.7	1.5	2.6

LM ratios of 40% and 20%, respectively, were determined. Based on previous research on foamed geopolymer materials, a ratio of 0.37 to the total amount of FA and SF was used for the WG [9]. A standard mortar with a sand-to-cement ratio of 2 and the same water-to-binder ratio was used for the RF sample.

The initial step involved blending the solid raw materials in a dry state, after which the sodium silicate solution was introduced and mixed for a duration of 1 min. This was followed by another 5 min of mixing subsequent to the addition of water and a superplasticizer, with the aim of achieving a uniform mixture. The fresh paste was then poured into a 50 × 50 × 50 mm^3 mold, which was sealed with plastic wrap and left at room temperature for 24 h. The specimens were demolded and cured in a standard water chamber at 22 ± 2.0 °C until the day of testing.

2.3. Testing methods

2.3.1. Compressive strength and density measurement

The 28-day compressive strength and density of the mortar specimens were measured following ASTM C109 [25] and ASTM C567 [26], respectively. The averages of the three replicates were then used as representative test results for the compressive strength and density tests.

2.3.2. CT scanning measurement

Computed tomography (CT) scans were performed to calculate the porosity of the 50 × 50 × 50 mm^3 mortar specimens. One representative specimen for each mix design was chosen for the CT scan analysis. The voxel size was 0.051 mm, and the detection conditions included 210 kV voltage and 200 A current. A 2-mm copper filter was integrated. After scanning, the images were reconstructed with VG Studio 2.2 software (Volume Graphics, Germany). With greater than 900 X–Y plane images, the porosities of the specimens were calculated.

ImageJ, Version 1.49, was used to process the images, which were converted to 8-bit grayscale resolution, as shown in Fig. 1(a) and cropped to a 45 mm × 45 mm region of interest (ROI). To reduce the noise in the images, Gaussian and Median (1 × 1) filters were used. Fig. 1(b) shows reconstructions of the microstructure created by segmenting the materials in the ROI using grayscale thresholding. This allows the mortar and air voids to be separated. The software was also used to stack the thresholded images of the air voids. Because small isolated clusters of voids or grain voxels are known to correspond to small isolated pores or noise effects [27], these were removed from the image before further analysis. To avoid being classified as pores, all features smaller than 0.5 mm in diameter were removed from the binary segmented data.

2.3.3. Setting time measurement

The setting time was investigated following ISO 9597:2008 [28] with a Vicat apparatus (Heungjin Testing Machine, South Korea). The initial setting time was determined when the Vicat needle failed to penetrate 5 mm from the bottom of the mold. The needle was then changed to another needle with an angular ring attachment for the final setting time test. The final setting time was determined when the Vicat needle failed to make an impression on the surface of the paste.

2.3.4. Isothermal calorimetry

The TAM air conduction calorimeter (TA Instruments, USA) with eight channels was used for the isothermal calorimetry test, following ASTM C1679 [29]. A fresh paste for the different mixes was prepared and poured into a glass ampoule. It was then transferred to the instrument. The heat flow was measured for up to 72 h, encompassing the main hydration heat evolution from the induction period to the stable period.

2.3.5. Thermogravimetric analysis (TGA)

Measurements for the TGA were taken using a TGA machine (Q500 TA instruments, USA). After the specimens were tested for compressive strength, the test chunks were used for

Table 2 – Mix design (kg/m^3).

Mixture ID	Binder					WG[a]	Sand	Water	SP[b]
	Cement	LM	MK	SF	FA				
RF	628.57	–	–	–	–	–			
40LM4SF	125.71	251.43	125.71	25.14	100.57	46.51	1257.1	314.29	12.57
30LM4SF	188.57	188.57							
20LM4SF	251.43	125.71	125.71	25.14	100.57	46.51			
20LM0SF			150.86	–		37.21			
20LM8SF			100.57	50.29		55.82			

[a] WG: water glass (sodium silicate solution).
[b] SP: superplasticizer.

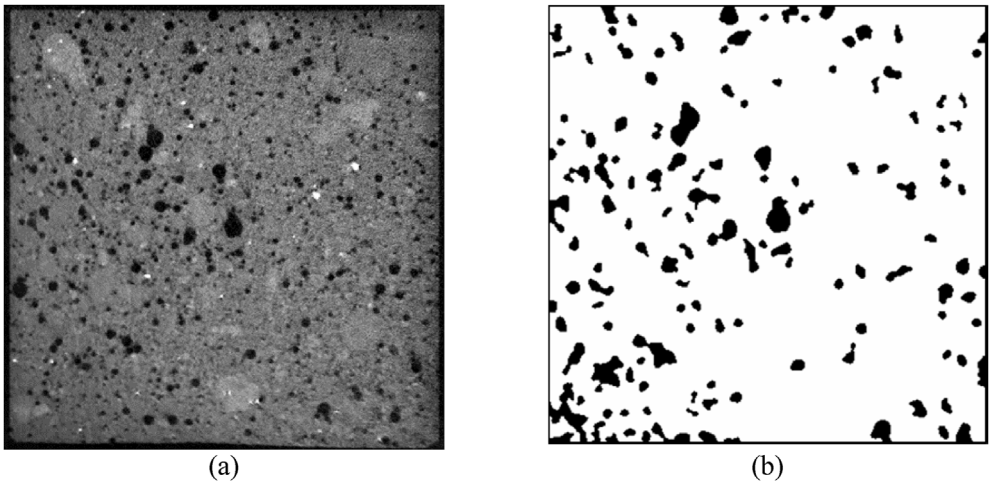

Fig. 1 – An example of the thresholding and filtering mortar specimen: (a) the original CT scan image and (b) the filtered and binarized image.

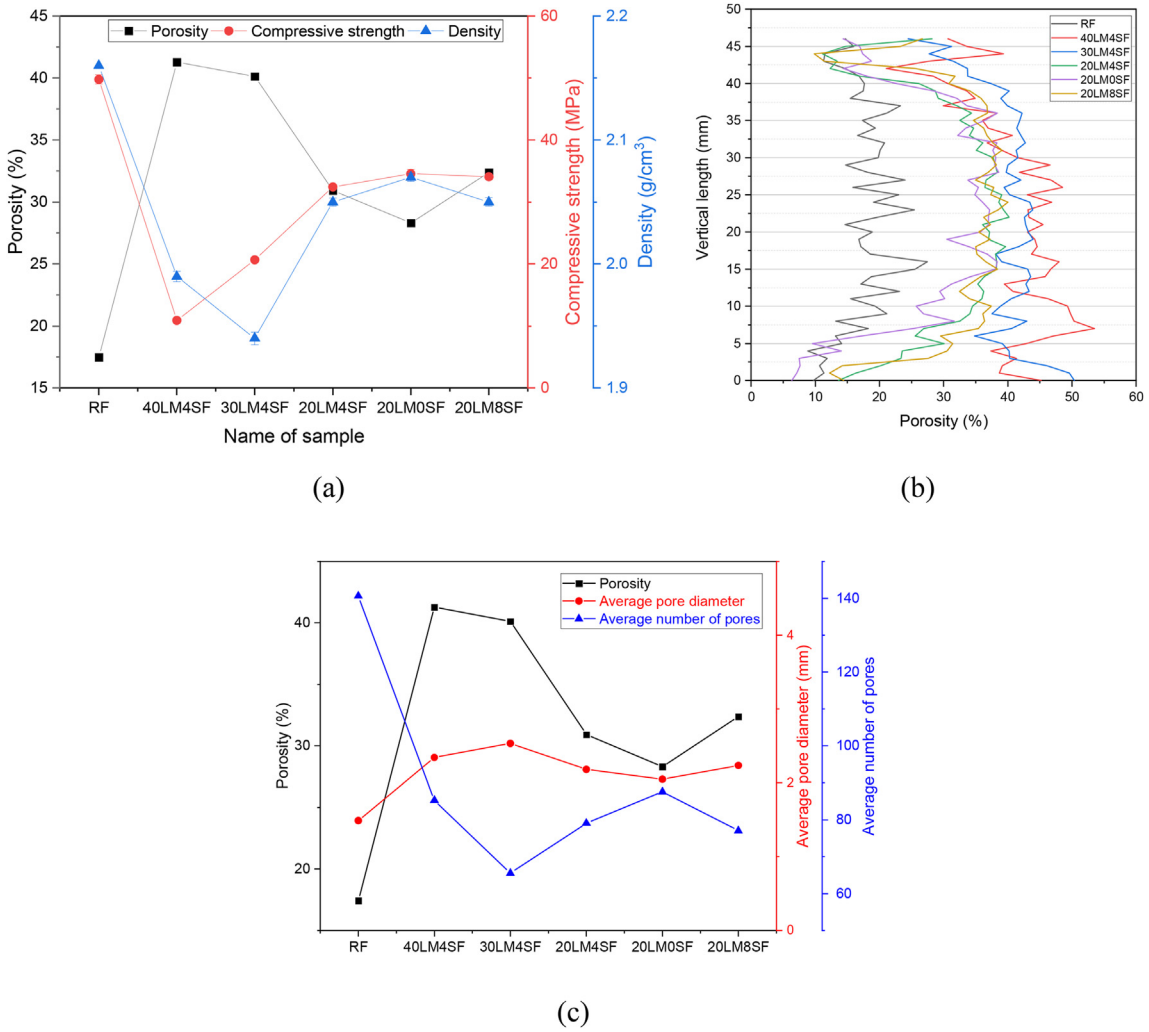

Fig. 2 – Porosity comparison of different blends: (a) the total porosity, density, and compressive strength; (b) the porosity distribution over the depth of the specimen; (c) the number of pores, the average pore diameter, and the porosity of the blends.

Table 3 – Comparison of CO2 emissions, compressive strength, porosity, and density of different blends.

	RF	C30 concrete	40LM4SF	30LM4SF	20LM4SF	20LM0SF	20LM8SF
Compressive strength (MPa)	49.79 ± 0.93	30	10.91 ± 0.23	20.66 ± 0.19	32.42 ± 0.67	34.55 ± 0.68	34.08 ± 0.71
CO_2 emission (kg CO_2 eq/tonne)	255	188	84	108	130	123	128
CO_2 emission efficiency (kg CO_2 eq/tonne/MPa)	5.12	6.27	7.70	5.23	4.01	3.56	3.75
Porosity (%)	17.48	–	41.28	40.13	30.92	28.31	32.38
Density (g/cm^3)	2.16 ± 0.0028	–	1.94 ± 0.0045	1.99 ± 0.0041	2.05 ± 00050	2.07 ± 0.0045	2.02 ± 0.0033

specimen preparation. The specimens were ground by the mortar and pestle. Then, the ground powder was immersed in isopropanol at a 10 ml/g ratio for 1 h to replace free water with isopropanol [30]. After the suspension was filtered and dried with a vacuum, the powder was dried further in an oven at 40 °C for 10 min before being stored in a desiccator until tested. The TGA was then run at a rate of 10 °C/min from 30 °C to 900 °C.

2.3.6. CO_2 emissions evaluation

The CO_2 emissions of each mixture were evaluated with SimaPro 9.3 software [31], a professional life cycle assessment tool widely used to evaluate CO_2 emissions. The Ecoinvent-3 library and the IMPACT world + Midpoint V1.01 evaluation method were used with this software for the assessment. To accurately determine the carbon footprint of each mixture, the materials used, and their production processes were considered. Moreover, for a fair comparison, the 30 MPa concrete was chosen as another reference specimen for use in CO_2 emissions evaluation (Section 3.5) because it has a similar compressive strength to most of the LMMGC specimens.

3. Results and discussion

3.1. Porosity analysis

The pore generation reaction of LMMGC is based on inorganic in situ foam formation theory. The pores might be caused by the hydrogen produced during the reduction reaction of water (Eq. (1)), silicon oxidation (Eq. (2)), and the formation of orthosilicic acid species (Eq. (3)) [9,32]:

$$4H_2O + 4e^- \rightarrow 2H_2 + 4OH^-, \quad (1)$$

$$Si^0 \rightarrow Si^{4+} + 4e^-, \quad (2)$$

$$4H_2O + Si^0 \rightarrow 2H_2 + Si(OH)_4. \quad (3)$$

The porosity, average pore diameter, and number of pores were the pore properties that were quantified using CT scans. These properties are commonly used to analyze the topology of porous media. The porosity was calculated as the volume of pores per unit of volume in the ROI. The average pore diameter was calculated using a thickness algorithm within the Particle

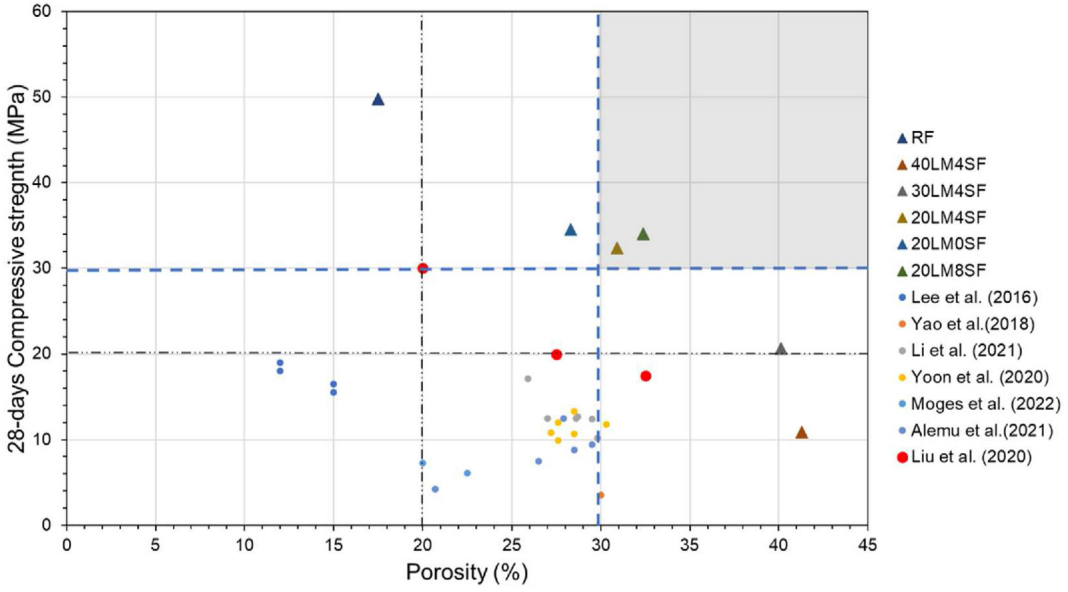

Fig. 3 – Porosity vs. compressive strength of mixtures in this study and previous studies [5–7,9,39–41].

Analyser plugin in ImageJ [33]. Furthermore, the average pore diameter, *Avd* (mm), was calculated as follows:

$$Avd = \frac{\sum_{i=1}^{n} d_i V_i}{\sum_{i=1}^{n} V_i}, \quad (4)$$

where d_i and V_i are the diameter and volume, respectively, of each pore within the ROI.

Using ImageJ software, the total porosity, porosity over depth, and average number of pores per scanned layer were measured, and the results show that more SF increased the pore formation. As shown in Fig. 2, pore formation was enhanced by a higher SF content. The porosity increased from 27% to 33% with only 8% SF, while a compressive strength above 30 MPa was maintained, as shown in Table 3 and Fig. 2(a). The main reason is that, as shown in Eq. (3), higher SF content results in a more sufficient foaming reaction with sodium silicate solution, which produces more H_2 gas, resulting in higher number of pores. In addition, higher LM content also increases porosity because a higher LM ratio reduces the amount of cement in the matrix and the number of hydration products, and affects the densification of the matrix, which corresponds to previous studies [20,34,35]. As can be seen in Fig. 2(a), the compressive strength and density results show that a higher amount of LM decreases the strength and density of the mortar. In addition, for all LMMGC specimens, the porosity increased as the density decreased.

Furthermore, as shown in Fig. 2(c), increasing the amount of SF from 4% to 8% did not significantly increase the porosity compared to the increase in the amount of SF from 0% to 4%. When the number of pores and the average diameter of the pores were compared, more SF increased the connectivity by reducing the number of pores. This has a positive effect on the material's sound absorption and damping properties [6,36,37]. In the case of LM, however, as shown in Fig. 2(a) and (c), the porosity increased sharply up to 30% LM and slightly up to 40%, indicating that there were more micropores up to 30% and macropores when 40% LM was used, which significantly degraded the strength of the blend.

3.2. *Compressive strength*

The compressive strength of all specimens after 28 days of water curing is shown in Fig. 3. Compared to the RF specimen, although the compressive strength of the LMMGC specimens decreased as the LM content increased, the compressive strength of most of the specimens with 20% LM was higher than 30 MPa, which can satisfy most construction applications. Significantly, when the LM content reached 40%, the compressive strength decreased to only 10.91 MPa, which decreased by 66% compared to the specimen containing 20% LM because of the low reactivity of the inactivated LM in the matrix [17,38]. The higher LM content increased the porosity of the specimens because it affected the matrix densification. This was discussed in Section 3.1.

The SF content slightly affected the compressive strength compared to the specimens with different LM content. As shown in Fig. 4, when the SF content increased to 8%, the compressive strength reached 34.10 MPa, which was slightly

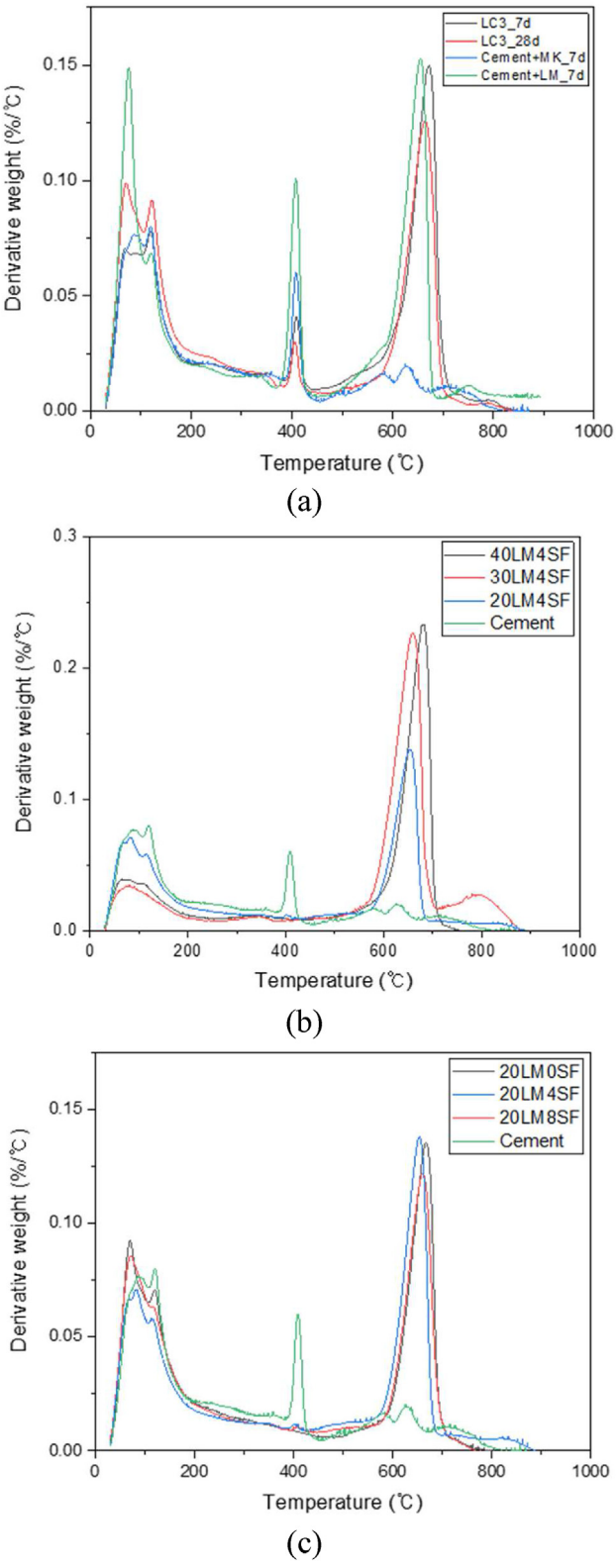

Fig. 4 – TGA comparison between different blends: (a) the reaction between LM and MK in LC^3 paste, (b) LMMGC specimens with different LM content, (c) LMMGC specimens with different SF content.

higher than the specimen with 4% SF content, but almost the same as the specimen without SF. This is because the higher SF content caused a more sufficient foaming reaction with the sodium silicate solution, leading to more pore generation, as discussed in Section 3.1. Meanwhile, sufficient SF can partially participate in the pozzolanic reaction; therefore, increasing the SF content to 8% can compensate for the decrement in compressive strength due to the increased porosity. This is discussed further in Section 3.3.

3.3. TGA

In this study, LM was used to replace limestone powder in the LC^3 paste, and the limestone powder was reactive with MK in a previous study [13]. Therefore, it is necessary to ascertain whether LM is reactive in the LC^3 specimens. They were prepared based on the mixing proportion of the 20LM4SF specimens after FA, SF, and sand were removed. As shown in Fig. 4(a), the specimen that contained only cement and MK did not have the calcite peak at 7 days due to the pozzolanic reaction, but the specimen that contained cement and LM had almost the same calcite peak as the LC^3 specimen at 7 days, which means the calcite peak of the LC^3 specimens occurred because of LM. Comparing the results of the 7- and 28-day LC^3 specimens, the calcite peak decreased at 28 days. This can be attributed to the slight reaction between MK and LM.

The TGA results for the LMMGC specimens with different LM content at 28 days are shown in Fig. 4(b). The peak between 100 °C and 200 °C of the specimen with 20% LM was the highest, and the calcite peak was the lowest among the three specimens because the specimen had the highest cement content and the lowest LM content. Moreover, portlandite did not exist in the specimens due to the pozzolanic reaction between pozzolanic materials and cement, and portlandite may transform into CSH gel. In addition, the portlandite might partially transform into CASH gel by the reaction between a fly ash–based geopolymer and cement [42].

The results for the LMMGC specimens with varied SF content are shown in Fig. 4(c). The results for the specimens were nearly the same. Only the first peak of the specimen that contained 4% SF was lower than those of the other specimens, whereas the calcite peak was slightly higher than those of the other specimens, which means less LM was reactive in the 20LM4SF specimen compared to the other specimens. The peak between 100 °C and 200 °C of the specimen with 8% SF was slightly higher than that of the 4% SF specimen, which means that the higher SF content might partially participate in the pozzolanic reaction.

3.4. Hydration kinetics

The setting time of six different blends was measured to evaluate the effects of LM and SF on the setting time. As can be seen in Fig. 5, when the amount of LM increased, the setting time was prolonged, especially for the specimen with 40% LM. Compared to other blends, the setting time was prolonged by 366%, almost 3 times longer than the 30LM4SF specimen. This could be due to the reaction between OH^- in the mortar system. In addition, the active silicon-aluminum phase in FA, named secondary hydration, may be promoted by the alkali in LM, thus partially offsetting the setting delay caused by the dilution effect. Moreover, the surface area of LM and SF was greater than that of the cement, resulting in less water in the matrix for the cement to hydrate. In the case of SF, the amount of the other materials was kept constant, and it can be seen that as SF increased from 0% to 8%, the setting time decreased by 1 h. This could be because SF performs better in an alkaline environment, and having LM provides more crystalline nuclei for the precipitation of hydration products.

Some changes were observed when the blend hydration kinetics were measured using the reaction heat. When the amount of LM increased, the induction period was prolonged, which corresponded to the setting time results. The delay effect of LM on the rate of heat evolution could be related to its chemical and physical effects on the cement hydration process. The water adsorption behavior of LM, SF, and FA due to their large specific surface area led to a decrease in the water that participated in the early cement hydration in cement

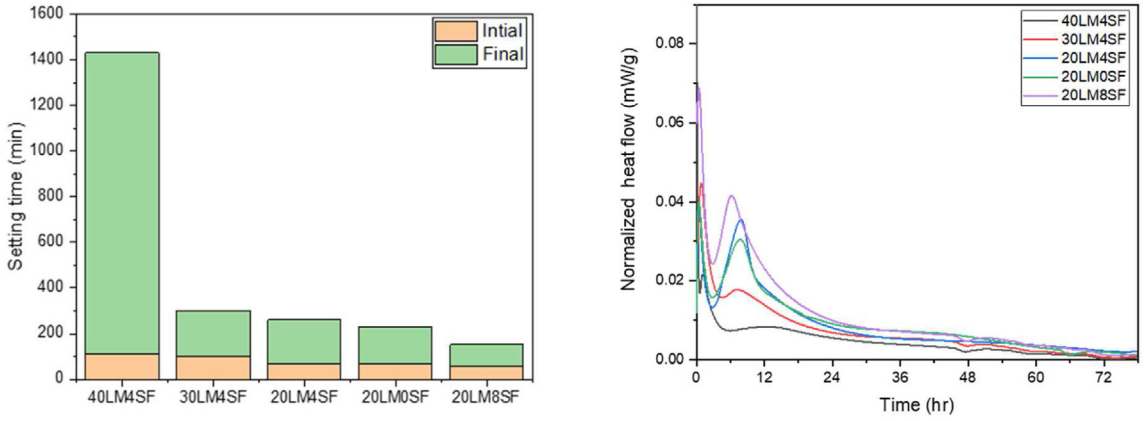

Fig. 5 – Setting time and hydration of different blends (a) setting time using Vicat; (b) hydration of the blends using isothermal calorimetry.

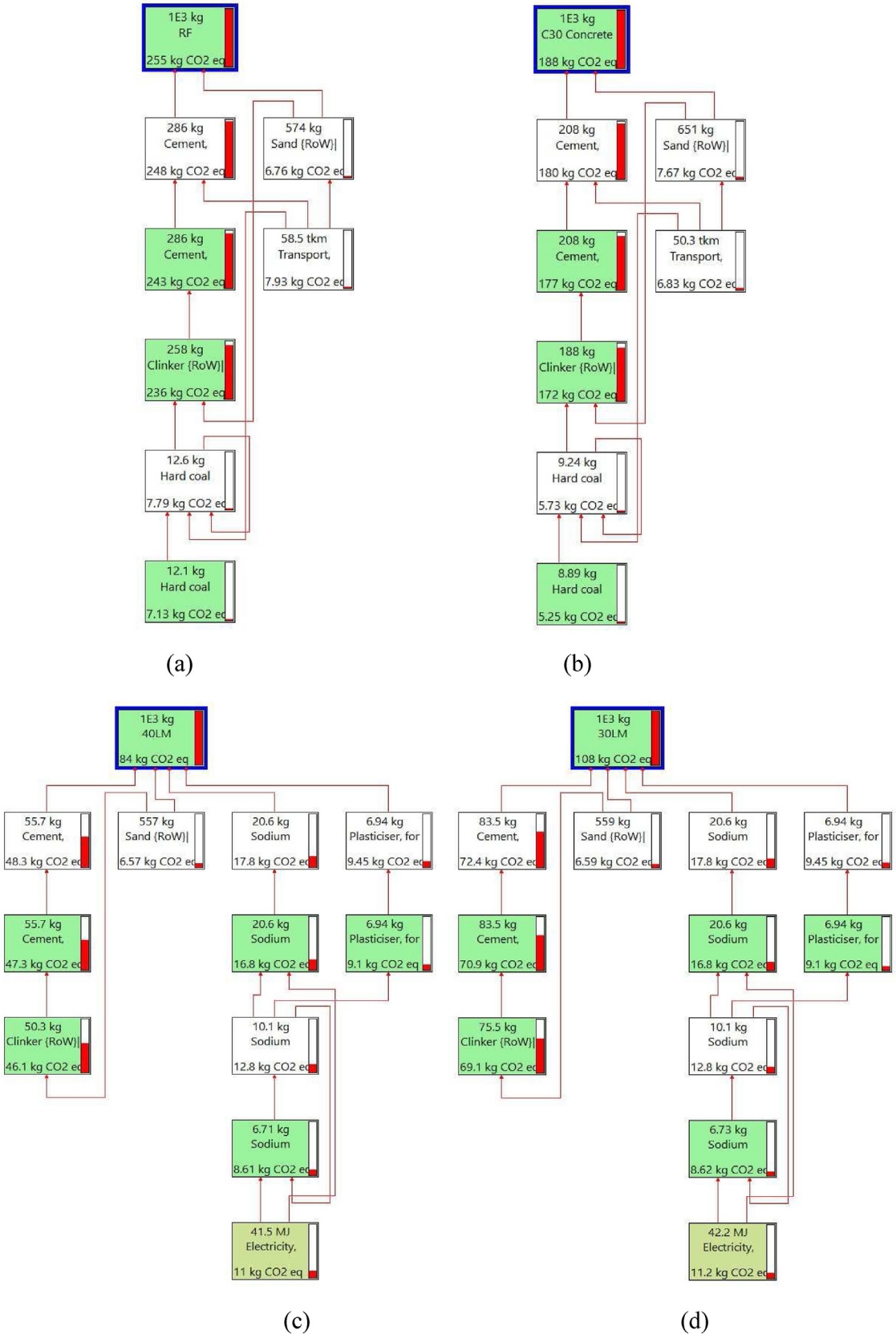

Fig. 6 – CO_2 emission evaluation flow chart of different mixtures: (a) RF, (b) C30 concrete, (c) 40LM4SF, (d) 30LM4SF, (e) 20LM4SF, (f) 20LM0SF, (g) 20LM8SF.

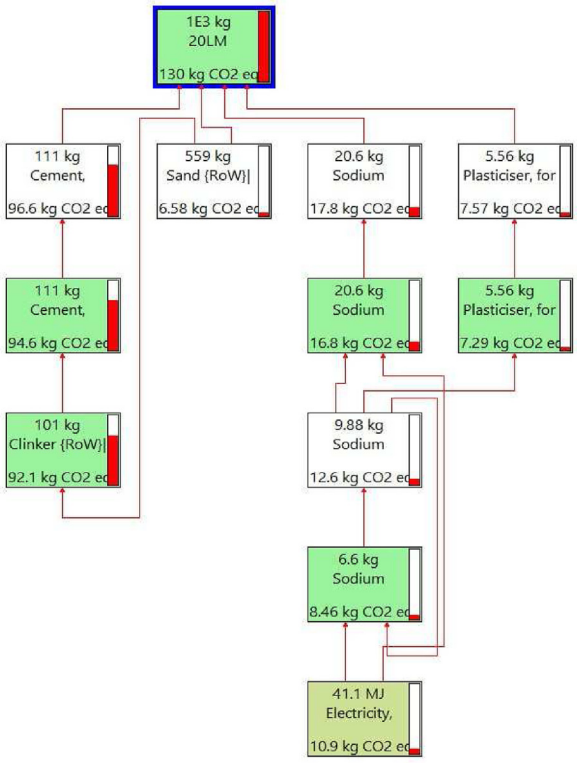

(e)

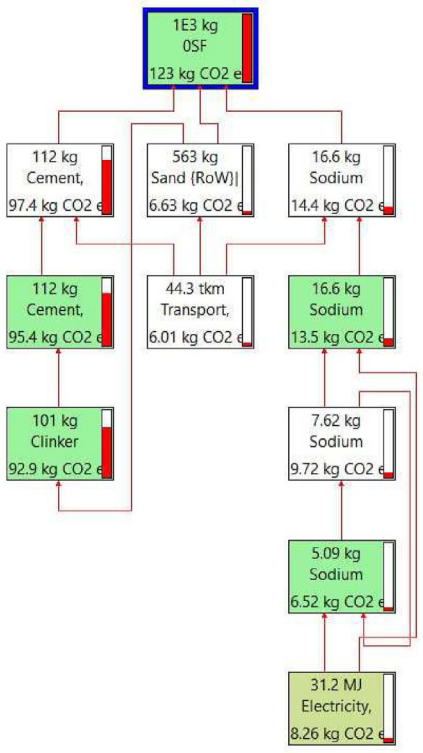

(f)

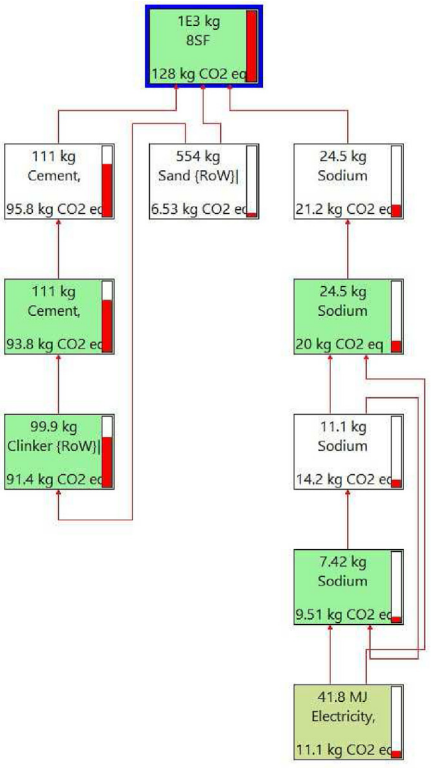

(g)

Fig. 6 – (*continued*).

paste [43,44], which caused limited hydration, and the delayed exothermic peak. It can be seen that the peaks of 20LM4SF and 20LM8SF were significantly higher than that of 40LM4SF, indicating that the more active SiO_2 in SF had been dissolved in the alkaline environment provided by LM [45], in which the active silicon-aluminum phase consumed OH^- to rapidly form CSH gel, thus having a high exothermic rate.

Furthermore, compared to other FA-based geopolymer paste setting times, the setting time of the LMMGC blends was nearly the same as that of the mortar containing SF, which shows that combining LC^3 and an FA-based geopolymer can solve this problem [46–48].

3.5. CO_2 emission evaluation

Fig. 6 illustrates the CO_2 emission evaluation flow chart of seven different mixtures, which includes the CO_2 emission of each material used in mixtures. The CO_2 emission evaluation results for each mixture are shown in Table 3 and Fig. 7. For a fair comparison, 30 MPa concrete (C30 concrete) was also chosen for comparison with the LMMGC mortar specimens, which has a similar compressive strength to most LMMGC mortar specimens. Compared to the RF specimen and 30 MPa concrete, the CO_2 emissions decreased with the increase in LM content. The CO_2 emissions of the specimen with 20% LM were 49.02% lower than that of the RF specimen and 30.85% lower than that of the 30 MPa grade concrete. In addition, CO_2 emission efficiency was used to evaluate CO_2 emissions for making 1 MPa material; therefore, lower CO_2 emission efficiency means fewer CO_2 emissions. CO_2 emission efficiency increased with the LM content, as shown in Table 3 and Fig. 7. The 20LM4SF specimen had the lowest CO_2 emission efficiency in terms of LM content, which decreased to 4.01.

Moreover, with the same LM content, the change of SF content hardly affected the CO_2 emissions due to the low SF content in the mix design. However, compared to the RF and 30 MPa grade concrete, the CO_2 emissions of the specimen that contained 8% SF (20LM8SF) decreased by 49.80% and 31.91%, respectively. The CO_2 emission efficiency of the specimen with 8% SF decreased to 3.75, which was 26.76% and 40.19% lower than that of the RF and 30 MPa concrete specimens, respectively. The specimen with 20% LM and 8% SF was a relatively better proportion in terms of CO_2 emission efficiency and porosity in this study. Furthermore, the LMMGC improved the utilization of industrial byproducts so that the CO_2 emissions decreased significantly. Therefore, the developed LMMGC can be defined as a low-carbon construction material.

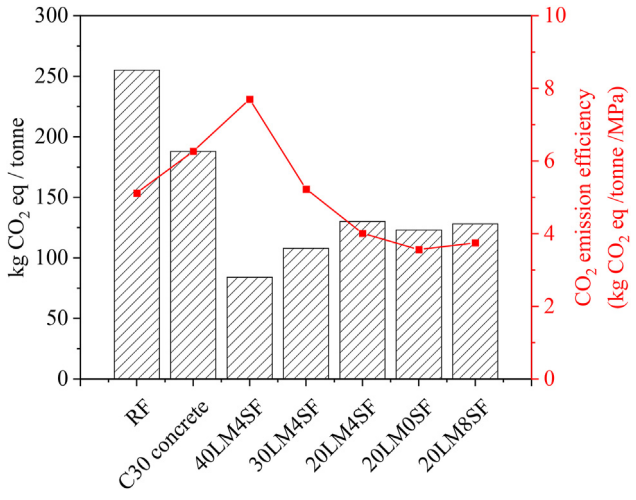

Fig. 7 – Comparison of CO_2 emissions and CO_2 emission efficiency.

4. Conclusion

This study aimed to use LC^3 with LM and a fly ash–based geopolymer mixed to develop the LMMGC (20LM8SF) that has more than 30% porosity and more than 30 MPa compressive strength. The curing limitation and rapid setting problems of conventional foamed fly ash–based geopolymers were solved for this material. Moreover, this material can enhance the utilization of industrial byproducts compared to normal construction materials so that CO_2 emissions can be reduced. The key observations and findings of this research can be summarized as follows:

1. Pore formation was aided by higher SF content; with only 8% SF, the porosity increased from 27% to 33%, while the compressive strength remained constant. In the case of the LM replacement, more LM increased porosity due to its effect on cement hydration, where more LM reduced the amount of cement in the matrix, the number of hydration products, and matrix densification, which can collaborate with the strength data.
2. The compressive strength of the specimens decreased with the LM content due to the low reactivity of LM. However, the compressive strength of the specimen with 20% LM content was still higher than 30 MPa. The SF content slightly affected the compressive strength of the specimen with the 8% SF content, because the higher SF content could partially participate in the pozzolanic reaction.
3. The TGA results showed that LM is reactive with MK in the LC^3 specimen. The portlandite was transferred into CSH and CASH gels because of the pozzolanic materials and geopolymer components in the specimens.
4. The setting time of six different blends was measured to evaluate how the amount of LM and SF affected the setting time. Although the alkali introduced by LM promoted secondary or further hydration of SF, it caused a setting time delay due to the dilution effect caused by the decrease in the amount of cement. When the amount of LM increased, the setting time was prolonged by 366%, particularly for the specimen with 40% LM, which was also seen in the heat of hydration test, which has a high induction period.
5. The CO_2 emissions of the LMMGC specimens decreased with the increase in lime mud. Compared to the RF specimen and the 30 MPa concrete, the CO_2 emissions of the LMMGC specimen with 20% LM and 8% SF decreased by 49.80% and 31.91%, respectively.

This experimental research proposed new high-strength foamed cementitious composites that have more than 30% porosity and more than 30 MPa compressive strength in a

sustainable way. However, additional research is needed to investigate and characterize additional merits, such as vibration reducibility and sound absorption capability.

Declaration of competing interest

The authors declare that they have no conflicts of interests.

Acknowledgment

This work was supported by the National Research Foundation of Korea (NRF) grant funded by the Korea government (MSIT) (No. 2021R1A4A1030867 and RS-2023-00212366). The opinions expressed in this paper are those of the authors and do not necessarily reflect the views of the sponsors or their employers.

REFERENCES

[1] Chen YX, Wu F, Yu Q, Brouwers HJH. Bio-based ultra-lightweight concrete applying miscanthus fibers: acoustic absorption and thermal insulation. Cement Concr Compos Nov. 2020;114. https://doi.org/10.1016/j.cemconcomp.2020.103829.

[2] Zhang Z, Provis JL, Reid A, Wang H. Mechanical, thermal insulation, thermal resistance and acoustic absorption properties of geopolymer foam concrete. Cement Concr Compos Jun. 2015;62:97–105. https://doi.org/10.1016/j.cemconcomp.2015.03.013.

[3] Oinam Y, Ju S, Gwon S, Shin M, Pyo S. Characteristics of GGBFS-Based Pervious Concrete Considering Rheological Properties of the Binder. Int J Concr Struct Mater 2022;16(1):1–14.

[4] Zhou C, Pei X, Li W, Liu Y. Mechanical and damping properties of recycled aggregate concrete modified with air-entraining agent and polypropylene fiber. Materials 2020;13(8). https://doi.org/10.3390/MA13082004.

[5] Yoon J, Kim H, Koh T, Pyo S. Microstructural characteristics of sound absorbable porous cement-based materials by incorporating natural fibers and aluminum powder. Construct Build Mater 2020;243:118167. https://doi.org/10.1016/j.conbuildmat.2020.118167.

[6] Moges KA, Park S, Pyo S. Sound absorption characteristics of surface perforated mortar with micro-sized pores. Appl Acoust Jun. 2022;195:108811. https://doi.org/10.1016/J.APACOUST.2022.108811.

[7] Alemu AS, Yoon J, Tafesse M, Seo YS, Kim HK, Pyo S. Practical considerations of porosity, strength, and acoustic absorption of structural pervious concrete. Case Stud Constr Mater 2021;15(November):e00764. https://doi.org/10.1016/j.cscm.2021.e00764.

[8] Arellano Aguilar R, Burciaga Díaz O, Escalante García JI. Lightweight concretes of activated metakaolin-fly ash binders, with blast furnace slag aggregates. Construct Build Mater Jul. 2010;24(7):1166–75. https://doi.org/10.1016/J.CONBUILDMAT.2009.12.024.

[9] Liu X, Hu C, Chu L. Microstructure, compressive strength and sound insulation property of fly ash-based geopolymeric foams with silica fume as foaming agent. Materials 2020;13(14). https://doi.org/10.3390/ma13143215.

[10] Luukkonen T, Abdollahnejad Z, Yliniemi J, Kinnunen P, Illikainen M. One-part alkali-activated materials: a review. Cement Concr Res July 2017;103:21–34. https://doi.org/10.1016/j.cemconres.2017.10.001. 2018.

[11] Jun Y, Han SH, Kim JH. Performance of CO2-cured alkali-activated slag pastes during curing and exposure. Int J Concr Struct Mater Dec. 2023;17(1). https://doi.org/10.1186/s40069-022-00563-3.

[12] Amir BM, Mehdi R. Evaluation of CO2 emissions reduction strategies in the Iranian cement industry. J Civ Eng Mater Appl 2021;5(3):107–14. https://doi.org/10.22034/jcema.2021.281049.1054. published by Pendar Pub.

[13] Sharma M, Bishnoi S, Martirena F, Scrivener K. Limestone calcined clay cement and concrete: a state-of-the-art review. Cement Concr Res Nov. 2021;149:106564. https://doi.org/10.1016/J.CEMCONRES.2021.106564.

[14] Avet F, Sofia L, Scrivener K. Concrete performance of limestone calcined clay cement (LC3) compared with conventional cements. Adv Civ Eng Mater 2019;8(3):275–86. https://doi.org/10.1520/ACEM20190052.

[15] Sthiannopkao S, Sreesai S. Utilization of pulp and paper industrial wastes to remove heavy metals from metal finishing wastewater. J Environ Manag 2009;90(11):3283–9. https://doi.org/10.1016/j.jenvman.2009.05.006.

[16] Nurmesniemi H, Pöykiö R, Keiski RL. A case study of waste management at the Northern Finnish pulp and paper mill complex of Stora Enso Veitsiluoto Mills. Waste Manag 2007;27(12):1939–48. https://doi.org/10.1016/j.wasman.2006.07.017.

[17] Vashistha P, Moges KA, Pyo S. Alkali activation of paper industry lime mud and assessment of its application in cementless binder. Dev Built Environ 2023;14:100146.

[18] Solahuddin BA, Yahaya FM. Properties of concrete and structural behaviour of reinforced concrete beam containing shredded waste paper as an additive. Int J Concr Struct Mater Apr. 2023;17(1):26. https://doi.org/10.1186/s40069-023-00588-2.

[19] Borinaga- Treviño R, Cuadrado J, Canales J, Rojí E. Lime mud waste from the paper industry as a partial replacement of cement in mortars used on radiant floor heating systems. J Build Eng Sep. 2021;41:102408. https://doi.org/10.1016/J.JOBE.2021.102408.

[20] Dong B, Chen C, Fang G, Wu K, Wang Y. Positive roles of lime mud in blended Portland cement. Construct Build Mater 2022;328:127067. https://doi.org/10.1016/j.conbuildmat.2022.127067. March.

[21] Scrivener K, Martirena F, Bishnoi S, Maity S. Calcined clay limestone cements (LC3). Cement Concr Res Dec. 01, 2018;114:49–56. https://doi.org/10.1016/j.cemconres.2017.08.017. Elsevier Ltd.

[22] Badogiannis E, Kakali G, Tsivilis S. Metakaolin as supplementary cementitious material : optimization of kaolin to metakaolin conversion. J Therm Anal Calorim 2005;81(2):457–62. https://doi.org/10.1007/s10973-005-0806-3.

[23] McLellan BC, Williams RP, Lay J, Van Riessen A, Corder GD. Costs and carbon emissions for geopolymer pastes in comparison to ordinary portland cement. J Clean Prod Jun. 2011;19(9–10):1080–90. https://doi.org/10.1016/j.jclepro.2011.02.010.

[24] ASTM C305. "Mechanical mixing of hydraulic cement pastes and mortars of plastic consistency,". Annu Book ASTM (Am Soc Test Mater) Stand 1998;14(2):147. https://doi.org/10.1177/089033449801400218.

[25] ASTM C109/109M-16a. "Standard test method for compressive strength of hydraulic cement mortars (Using 2-

in. or cube specimens), vol. 4. Annual Book of ASTM Standards; 2016. p. 1–10. https://doi.org/10.1520/C0109.
[26] ASTM C567/C567M-19. Standard test method for determining density of structural lightweight concrete. April ASTM International 2019;4:4–6. https://doi.org/10.1520/C0567.
[27] Peth S, Horn R, Beckmann F, Donath T, Fischer J, Smucker AJM. Three-dimensional quantification of intra-aggregate pore-space features using synchrotron-radiation-based microtomography. Soil Sci Soc Am J 2008;72(4):897–907. https://doi.org/10.2136/sssaj2007.0130.
[28] ISO 9578:2008. Cement — Test methods — Determination of setting time and soundness2008; 2008.
[29] ASTM C1679-14. Standard practice for measuring hydration kinetics of hydraulic cementitious mixtures using isothermal calorimetryvol. 4. Annual Book of ASTM Standards Volume 04; 2014. p. 16. https://doi.org/10.1520/C1679-17.2. 01.
[30] Scrivener K, Snellings R, Lothenbach B. A practical guide to microstructural analysis of cementitious materials62; 2016. 10.
[31] Mark Goedkoop EM, Oele Michiel, Vieira Marisa, Leijting Jorrit, Ponsioen Tommie. SimaPro Tutorial Colophon. May, 2014.
[32] Prud'homme E, Michaud P, Joussein E, Peyratout C, Smith A, Arrii-Clacens S, et al. Silica fume as porogent agent in geo-materials at low temperature. J Eur Ceram Soc May 2010;30(7):1641–8. https://doi.org/10.1016/J.JEURCERAMSOC.2010.01.014.
[33] Aboufoul M, Garcia A. Factors affecting hydraulic conductivity of asphalt mixture. Mater Struct/Materiaux et Constructions 2017;50(2):1–16. https://doi.org/10.1617/s11527-016-0982-6.
[34] Moges KA, Pyo S. Effect of high replacement ratio of lime mud as a filler on mechanical and hydration properties of high-strength mortar. Construct Build Mater Aug. 2023;392. https://doi.org/10.1016/j.conbuildmat.2023.131974.
[35] Modolo RCE, Senff L, Labrincha JA, Ferreira VM, Tarelho LAC. Lime mud from cellulose industry as raw material in cement mortars. Mater Construcción Oct. 2014;64(316). https://doi.org/10.3989/mc.2014.00214.
[36] Abhilasha, Kumar R, Lakhani R, Mishra RK, Khan S. Utilization of solid waste in the production of autoclaved aerated concrete and their effects on its physio-mechanical and microstructural properties: alternative sources, characterization, and performance insights. Int J Concre Struct Mater Dec. 01, 2023;17(1). https://doi.org/10.1186/s40069-022-00569-x. Springer Nature Korea.
[37] Wu S, Park S, Pyo S. Effect of types of microparticles on vibration reducibility of cementitious composites. Materials 2022;15(14). https://doi.org/10.3390/ma15144821.
[38] Azgomi F. Impact of liming ratio on lime mud settling and filterability in the kraft recovery process. 2014.
[39] Lee J-W, Jang Y-I, Park W-S, Kim S-W. A study on mechanical properties of porous concrete using cementless binder. Int J Concr Struct Mater 2016;10. https://doi.org/10.1007/s40069-016-0166-3.
[40] Yao A, Ding H, Zhang X, Hu Z, Hao R, Yang T. Optimum design and performance of porous concrete for heavy-load traffic pavement in cold and heavy rainfall region of NE China. Adv Mater Sci Eng 2018;2018. https://doi.org/10.1155/2018/7082897.
[41] Li LG, Feng J-J, Xiao B-F, Chu S-H. Experimental study on porosity, permeability and strength of pervious concrete. 2021. p. 1–26.
[42] Park S, Moges KA, Wu S, Pyo S. Characteristics of hybrid alkaline cement composites with high cement content: flash set and high compressive strength. J Mater Res Technol 2022;17:1582–97. https://doi.org/10.1016/j.jmrt.2022.01.105.
[43] Langan BW, Weng K, Ward MA. Effect of silica fume and fly ash on heat of hydration of Portland cement. Cement Concr Res Jul. 2002;32(7):1045–51. https://doi.org/10.1016/S0008-8846(02)00742-1.
[44] Yogendran V, Langan BW, Ward MA. Hydration of cement and silica fume paste. Cement Concr Res Sep. 1991;21(5):691–708. https://doi.org/10.1016/0008-8846(91)90164-D.
[45] Mehta A, Ashish DK. Silica fume and waste glass in cement concrete production: a review. J Build Eng May 2020;29:100888. https://doi.org/10.1016/J.JOBE.2019.100888.
[46] Chindaprasirt P, De Silva P, Sagoe-Crentsil K, Hanjitsuwan S. Effect of SiO 2 and Al 2O 3on the setting and hardening of high calcium fly ash-based geopolymer systems. J Mater Sci 2012;47(12):4876–83. https://doi.org/10.1007/s10853-012-6353-y.
[47] Rattanasak U, Pankhet K, Chindaprasirt P. Effect of chemical admixtures on properties of high-calcium fly ash geopolymer. Int J Miner Metall Mater 2011;18(3):364–9. https://doi.org/10.1007/s12613-011-0448-3.
[48] Antoni A, Herianto JG, Anastasia E, Hardjito D. Effect of adding acid solution on setting time and compressive strength of high calcium fly ash based geopolymer. AIP Conf Proc 2017;1887. https://doi.org/10.1063/1.5003525.